LAWRENCE
LIVERMORE
NATIONAL
LABORATORY

LLNL-JRNL-853782

TATB thermal decomposition: Expanding the molecular profile with cryo-focused pyrolysis GC-MS

K. D. Morrison, J. S. Moore, K. R. Coffee, B. Koroglu, A. K. Burnham, J. G. Reynolds

August 30, 2023

Propellants, Explosives, Pyrotechnics

Disclaimer

Propellants,
Explosives,
Pyrotechnics

Research Article

LLNL-JRNL-853782

DOI: 10.1002/prep.201((full DOI will be filled in by the editorial staff))

TATB thermal decomposition: Expanding the molecular profile with cryo-focused pyrolysis GC-MS

Keith D. Morrison*[a], Jason S. Moore[a], Keith R. Coffee[a], Batikan Koroglu[a], Alan K. Burnham[b], John G. Reynolds[a]

Abstract: Understanding the molecular composition of high explosives during thermal decomposition is vital for predicting the sensitivity, safety, and performance of explosive materials. The thermal decomposition of 1,3,5-triamino-2,4,6-trinitrobenzene (TATB) has been linked to the formation of furazans through a series of dehydration reactions of the NO_2 and NH_2 groups on the phenyl ring, along with breakdown into small molecules (≤ 120 amu). Molecular identification of compounds formed in this transformation of the furazans to light gases has been lacking. To address this, we have applied a pseudo-confined sampling system in a cryo-focused pyrolysis gas chromatography-mass spectrometry (pyGC-MS) system to molecularly identify these intermediates. By design, sublimation of TATB, which has complicated MS analyses of thermal degradation, was significantly reduced and additional compounds were identified with potential structural information. In addition to the known furazan compounds, one of these compounds forms from the loss of oxygen from benzo-trifurazan (F3) and produces an open ring structure that may be the first step in the formation of lower molecular weight furazan breakdown products. The loss of a nitro group from benzo-monofurazan (F1) was also discovered and implicates the formation of oxidizing NO_2 gas in the thermal decomposition mechanism. These findings are vital for understanding the proper heat flow from energetic materials on a molecular level, necessary when measuring enthalpy and developing decomposition models based on kinetic parameters.

Keywords: TATB · thermal decomposition · pyrolysis GC-MS · explosives

1 Introduction

Understanding the molecular composition of high explosives during thermal decomposition is vital for predicting their sensitivity, safety and performance [1]. TATB is one such explosive because of the extended use in munitions [2]. First synthesized in 1886 [3], the structural features of TATB have attracted much attention [4]. The compound has a fully substituted benzene ring with alternating amino- and nitro-group substituents, crystallizes into almost planar sheets which stack to form a tertiary structure, held together by hydrogen bonding, both inter- and intra-molecular. The tertiary structure dictates properties such as solubility [5] and initiation of decomposition [6], while the substituents on the ring dictate molecular reactivity [7]. Studies on the gas-phase thermal decomposition of TATB have traditionally relied on the use of a Langmuir vacuum cell coupled to a quadrupole mass spectrometer, or the more modern simultaneous DSC/TGA quadrupole mass spectrometers (SDT-MS) with vacuum or gas flow cells [8-12]. The majority of studies on TATB thermal decomposition have found that several species of light gases (CO_2, N_2, NO, N_2O, NO_2, NH_3) and water vapor form as TATB is heated to decomposition temperatures (300-400°C) [8, 9, 11-13]. Additionally, a series of furazan compounds sequentially form with F_1 (benzo-monofurazan), F_2 (benzo-difurazan) and F_3 (benzo-trifurazan) observed in numerous studies [7-9, 11-16]. The evolved gas analysis (EGA) of TATB thermal breakdown coupled with the gravimetric and heat flow results provide a powerful tool to decouple the thermal and molecular processes that drive the decomposition of TATB. While these analytical techniques have generated a wealth of information on TATB thermal processes, they do not offer any separation and verification of distinct molecules that are contributing to the decomposition mechanism. Mass spectrometry techniques that combine chromatographic separation of molecules with thermal analysis of evolved gases can bolster our understanding of TATB thermal decomposition mechanisms.

Pyrolysis GC-MS is an analytical technique that can be used to measure gases evolved from solid samples as they are heated in a furnace purged with an inert gas (helium). Traditional pyGC-MS systems required manual insertion of samples and were mostly limited to flash pyrolysis (>600°C, 5-10 seconds) conditions to acquire chromatographic separation of compounds [17]. Modern pyGC-MS systems are equipped with autosamplers, multi-stage heating furnaces with automated sample removal and insertion over programmed temperature ranges, along with cryogenic focusing of compounds for chromatography collected over minutes to hours [18].

This study investigates the thermal decomposition of TATB using pyGC-MS in EGA mode aided by cryo-focused chromatography, which allowed us to discern the molecular processes occurring as TATB encounters elevated temperatures. The results represent typical production purity TATB synthesized by the wet-amination method. Our findings reveal several overlooked molecular species involved in the thermal decomposition of TATB. These findings aided

[a] *Keith D. Morrison*, Jason S. Moore, Keith R. Coffee, Batikan Koroglu, John G. Reynolds.*
Lawrence Livermore National Laboratory
7000 East Avenue, Livermore, CA 94550
E-mail: morrison30@llnl.gov

[b] *Alan K. Burnham. Stratify//MH Chew Associates*
7633 Southfront Road, Ste. 170, Livermore, CA 94551

Supporting information for this article is available on the WWW under http://www.pep.wiley-vch.de or from the author.

in the development of a robust global kinetic decomposition model that incorporates more complex molecular processes and reactions [19]. These finding will aid in our understanding of nitro-amine based explosives and better help predict the consequence of exposure to abnormal thermal environments.

2 Experimental Section

2.1 TATB Samples

TATB was synthesized via the wet-amination process [20] with additional steps to remove ammonium chloride impurities [21]. All samples were verified for purity following established methods [22] and found only trace impurities of T4A (1-chloro-3,5-dinitro-2,4,6-triaminobenzene, 0.028 wt.%) and FX1 (benzo-monofuroxan, 0.005 wt. %) [22].

2.2 Unconfined and pseudo-confined sample preparation

The analysis of TATB thermal decomposition processes can be confounded due to sublimation, resulting in the volatilization of TATB molecular ions instead of thermal decomposition products [23]. TATB thermal decomposition measurements using DSC/TGA revealed that pseudo-confined sample pans with 50-75 µm pinhole openings mostly eliminated TATB sublimation into the gas phase, allowing thermal decomposition processes and accurate measurement of heat flow and enthalpy [23].

The Frontier pyGC-MS system and autosampler do not offer sample cups with pinhole openings, so we devised a method to introduce consistent confinement of the TATB using silver foils. Figure 1 shows the sample cups (Frontier Eco-Cups) and the quartz wool and silver foil cups used to prepare confined and pseudo-confined TATB. This allowed us to study the thermal decomposition of TATB in both unconfined and pseudo-confined environments that are analogous to the DSC/TGA experiments in the literature. For unconfined samples, TATB powders (200-350 µg) were loaded into the bottom of the cups and a quartz disc was placed on top of the powder, followed by quartz wool (Figure 1A and B). The quartz disc and wool are needed to prevent the scattering of TATB particles on the furnace wall when the sample is being loaded and ejected from the autosampler. The quartz wool produces minimal confinement of gases during heating and represents unconfined conditions. Pseudo-confined samples were prepared using silver foil cups (Costech silver capsules 5 x 9 mm, 40 mg) and a standardized folding and compression routine to restrict free gas flow and produce consistent EGA results (Figure 1C).

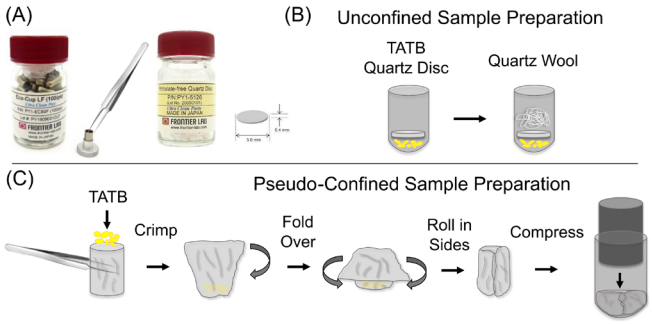

Figure 1. Unconfined and pseudo-confined sample preparation. (A) Frontier steel sample cups used to prepare unconfined and pseudo-confined TATB samples for thermal analysis. (B) Preparation of unconfined TATB samples using quartz discs and wool. (C) Standardized folding and compression method to prepare pseudo-confined TATB samples using silver foil cups.

2.3 Pyrolysis GC-MS system

The EGA and pyrolysis GC-MS experiments were performed using an Agilent 7890B GC coupled to a 7010B MS/MS mass spectrometer electron impact ionization (EI). The Frontier Lab multi-function pyrolysis system was installed on the back inlet of the GC oven. This system uses the multi-shot pyrolyzer (EGA/PY-3030D), auto-shot sampler (AS-2020E), selective sampler (SS-2010E) and microjet cryo-trap (MJT-1035E). The TATB samples were analyzed in either EGA mode (no chromatographic separation) or cryo-focused pyGC-MS mode (with chromatographic separation). Results were processed using Frontier Laboratories F-search (Version 3.6.3) and Agilent Mass Hunter Qualitative Analysis (Version 10.0) and the NIST GC-MS database (NIST v20).

The furnace on the Frontier multi-shot pyrolyzer was calibrated according to the manufacturer's recommendations using a thermocouple inserted into the furnace with a sample cup. The calibration was done across a temperature range from 100 to 650 °C and resulted in an average temperature difference of ± 0.2°C. Isothermal temperature stability was also measured to determine if fluctuations in furnace voltages resulted in oscillations in temperatures over time. The furnace was able to maintain isothermal temperatures (320-340 °C) range with < ± 0.035 °C variation over 10 min.

2.4 Evolved Gas Analysis GC-MS

Samples were analyzed in EGA mode using both pseudo-confined and un-confined sample preparation methods. The TATB samples were analyzed using the multi-shot pyrolyzer, auto-shot sampler, and selective sampler. An EGA steel column (3-meter x 150-µm inside diameter) with no stationary phase was used to direct evolved gases with no chromatographic separation into the mass spectrometer. Samples were measured in ramped heating mode starting at a temperature of 50 °C (1-min hold) and then heated at a rate of 10 or 5 °C/min to 600 °C. Isothermal experiments

were also performed at 330 °C for 100 min. The GC oven was kept at 300 °C during EGA analysis. Helium was used as the carrier gas for all experiments and the collision cell in the 7010B mass spectrometer used N_2 gas. Helium pressure on the EGA column was set at 116.87 kPa in constant pressure mode with a flow rate of 1 mL/min. The inlet to the GC-MS was kept at 300 °C and the septum purge flow was 3 mL/min. The inlet was run in split mode, with the gases entering the EGA column at a split flow of 50:1 (He : sample gas). The mass spectrometer was set to scan on the first quadrupole mass spectrometer from mass 29 to 650, using a 600-ms scan time.

2.5 Cryo-focused pyrolysis GC-MS

Samples were analyzed in cryo-focused pyrolysis GC-MS mode using silver foil pseudo-confined sample preparation methods. The TATB samples were analyzed using the multi-shot pyrolyzer, auto-shot sampler, selective sampler, and microjet cryo-trap in cryo-focused analysis mode. In this mode, gases were cryo-focused from isothermal experiments (330 °C) at 5-25 min and 25-45 min. Helium was used as the carrier gas for all experiments and the collision cell in the 7010B mass spectrometer used N_2 gas. An Agilent HP-5MS-UI (30-m x 250-µm inside diameter x 0.25-µm inner coating) column was installed and fed through the liquid nitrogen cryo-focusing coil to capture the evolved gases on the column for chromatographic separation. After the sample heating routine finished, the liquid nitrogen flow was shut off and the gases trapped in the column were heated for traditional GC-MS analysis. The GC oven was held at 40 °C for two min (after the cryogen flow was stopped), then heated at 20 °C/min to 320 °C, and then held for 15 min. Helium pressure was set to 61.36 kPa in variable pressure mode with a flow rate of 1 mL/min. The mass spectrometer was set to scan on the first quadrupole mass spectrometer from mass 15 to 650, using a 300-ms scan time.

3 Results

3.1 Thermal EGA analysis of TATB in unconfined and pseudo-confined environments

The preliminary EGA analysis of TATB thermal breakdown was done with 50-80 µg of sample loaded into unconfined steel cups with quartz wool. These masses were insufficient to measure TATB thermal decomposition at temperatures above 300 °C due to the rapid sublimation and decomposition of the explosive at temperatures above 350 °C (Figure S1). Additionally, samples analyzed without quartz wool produced erratic EGA chromatograms with peak scattering due to particle contamination of the quartz furnace tube (Figure S2). Masses of 200 to 350 µg provided enough sample to capture reproducible thermal events in the gas phase for unconfined and pseudo-confined TATB.

Figure 2A shows the total ion chromatogram (TIC) for replicate runs on unconfined samples at a 10 °C/min heating rate. The profiles essentially overlay with maximum gas evolution (T_{max}) values of 377.8 °C exhibiting excellent reproducibility. The production of gas-phase products increases at 330 °C in both the unconfined and pseudo-confined samples (Figure 2A and B). The ramped heating of pseudo-confined TATB at 10 °C/min produced T_{max} values of 382.4 °C (± 1.1 °C). When DSC/TGA measurements of TATB samples were run in pseudo-confined pans with 50-µm pinhole openings, the T_{max} values corresponding to the maximum heat flow and maximum rate of weight loss were 383.6 °C and 384.2 °C, respectively [23]. These values are in good agreement with the silver foil pseudo-confined samples and only differ by 1.2 to 1.8 °C. The differences in temperature are likely due to variations in heat flow in the sample holder and the degree of confinement. The silver foil pseudo-confinement method provides results that are directly comparable to the thermal profiles measured using calorimetry and facilitates multiple pyrolysis GC-MS methods. The ramped EGA profiles of pseudo-confined TATB produced 1.5 times greater amounts of gas-phase products (integration from 20-40 min) when compared to the unconfined TATB samples (Figure 2A and B). This is likely due to minimizing the TATB sublimation that occurs at temperatures > 300 °C [23], which leaves more TATB available for gas-phase thermal decomposition reactions. The rate of gas evolution during ramped heating increased at 330 °C for both unconfined and confined experiments regardless of the heating rate, indicating that temperatures ≥ 330 °C correlate with the onset of TATB thermal decomposition.

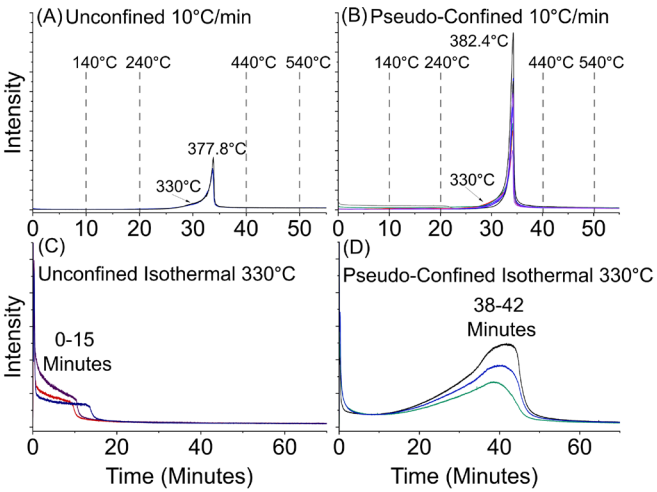

Figure 2. EGA total ion chromatograms (TIC) during ramped and isothermal heating of TATB using unconfined and pseudo-confined samples. (A) Unconfined EGA chromatograms and (B) pseudo-confined EGA chromatograms measured from 50-600 °C with a 10 °C/min heating ramp. (C) TATB EGA chromatograms during isothermal heating at 330 °C with (C) unconfined and (D) pseudo-confined samples. The TICs in the ramped heating (A-B) and isothermal plots (C-D) are all set to the same intensity scale, respectively.

Figure 2C shows the EGA profile for unconfined TATB heated isothermally at 330 °C. After an initial pulse of gases upon insertion of the sample, gas

generation reached baseline levels after 10 to 15 min of reaction. Figure 2D shows the pseudo-confined samples at isothermal conditions. After an initial pulse appears, the evolution decreases for a while reaching a steady state for about 10 min, but increases again to a maximum of evolution in the range of 38 to 42 min. At 60 min the production of gases decreases to baseline levels. The profiles are the same shape, but different intensities because of sample size. These differences in profile behavior can be explained by the sample cup design for which the pseudo-confined cup design favors decomposition over sublimation and is discussed below. The thermal profiles of the pseudo-confined isothermal TATB (Figure 2D) were reproducible when compared to the unconfined samples (Figure 2C).

3.2 EGA Mass Spectra of TATB

The EGA method does not employ any separation prior to MS detection so the results are a complex mixture of ions from molecular ions and fragments from EI ionization (70 eV). Figure 3A shows the spectrum of the unconfined TATB heated at 10 °C/min. The TATB molecular ion, m/z 258, has moderate intensity. The most intense peak in the mass spectrum is m/z 44, which represents the production of CO_2 or N_2O. The next most intense ion is m/z 52 followed by m/z 68. A series of higher molecular weight ions m/z 240, 228, 222, 177, 164 and 120 are also observed. Figure 3B shows the spectrum of pseudo-confined sample at 10 °C/min heating rate. The TATB molecular ion at m/z 258 is visible, but at much lower intensity than in Figure 3A, indicating the pseudo-confined environment minimizes sublimation during heating. In this case, fragment ions of TATB contribute very little to the overall masses observed. The unconfined and pseudo-confined TATB spectra are similar. However, m/z 177, 188 and 222 intensities were elevated in the pseudo-confined samples during heating. Figure 3C shows the spectrum of TATB when heated isothermally at 330 °C in an unconfined cup. Masses associated with furazan thermal breakdown products, m/z 240, 222, 204, are more intense relative to the TATB molecular ion. Figure 3D shows the spectrum of pseudo-confined TATB heated isothermally at 330 °C. Major peaks at m/z 44, 52, 68, 84, 90, 120 177, and 204 are apparent. The molecular ion of TATB is present as only a minor peak, indicating most of the TATB does not survive during heating at 330 °C and more complete thermal decomposition reactions are occurring.

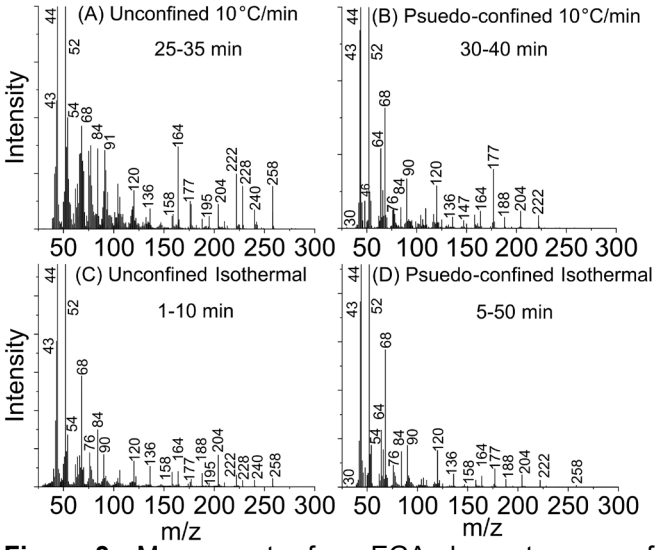

Figure 3. Mass spectra from EGA chromatograms of (A) unconfined and (B) pseudo-confined TATB during ramped heating from 50-600 °C at 10 °C/min. EGA chromatograms and mass spectra of isothermally heated TATB at 330 °C measured in an (C) unconfined or (D) pseudo-confined environment. All mass spectra have been re-scaled to focus on lower intensity ions. EGA mass spectrum time ranges are listed in minutes (See Figure 2 for EGA chromatograms).

3.3 Cryo-focused pyrolysis GC-MS analysis of TATB during isothermal heating

Further analysis of TATB thermal decomposition focused on pseudo-confined samples and isothermal heating (330 °C) to distinguish early versus late thermal decomposition processes (Figure 4).

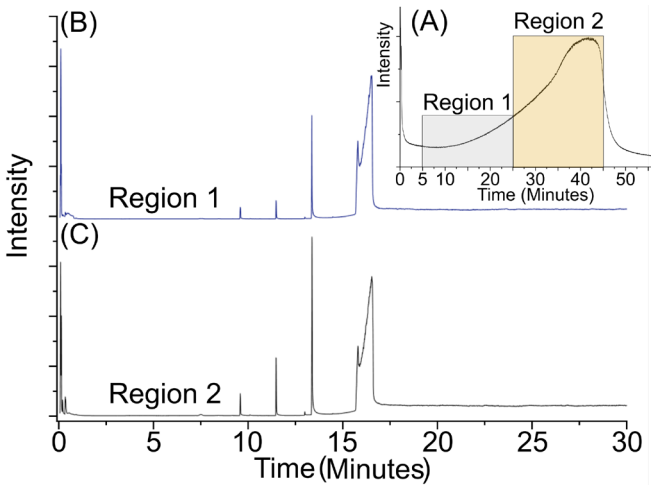

Figure 4. Cryo-focused GC-MS of isothermal TATB breakdown products in a pseudo-confined environment. (A) Regions used for cryo-trapping of evolved gases during isothermal heating at 330 °C. Chromatographic separation of cryo-focused compounds from (B) region 1 (5-25 min) and (C) region 2 (25-45 min).

Cryo-focused pyrolysis GC-MS allowed us to capture the distinct molecular species that produce the complex EGA mass spectra and separate them using chromatography. Figure 4A shows the two regions that

were selected for cryo-focused analyses. Region 1 (5-25 min) represents the reactions occurring in the steady-state gas evolution phase, and Region 2 (25-45 min) represents the increasing gas evolution phase. The total ion chromatogram from Region 1 produced 9 peaks above the background, while Region 2 had 11 resolved peaks (Figure 4B and C). The intensities of these peaks differ significantly and indicate different molecular processes occur with time as TATB is heated to decomposition temperatures. Preliminary compound structures have been assigned to each peak in the chromatogram based on previous studies and analysis of GC-MS fragmentation patterns (Figures 5-7).

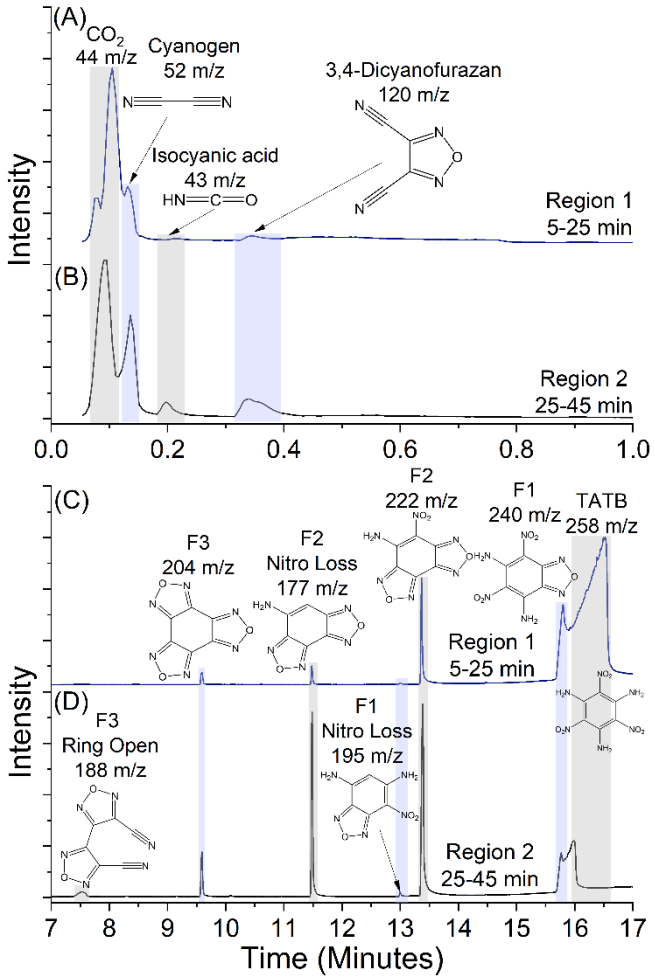

Figure 5. Total ion chromatograms of cryo-focused compounds identified during isothermal heating of TATB. Compounds retained in the first minute of the chromatogram (A and B) and compounds retained from 7-17 min (C and D) are displayed for cryo-focused Region 1 (5-25 min) and Region 2 (25-45 min).

Figure 5 shows the total ion chromatograms and molecular identification of the compounds eluted using the cryo-focusing. Figure 5A and B are the first eluting compounds of each cryo-focused Region 1 and 2, respectively. The chromatograms from 0-1 min have peaks ≤ m/z 120, representing molecular ions at mass 120, 52, 44 and 43. The first peak in the chromatogram represents CO_2, followed by cyanogen, isocyanic (or potentially isofulminic acid) and 3,4-dicyanofurazan. The separation of CO_2 was variable from sample to sample. This effect can be observed in Figure 5A, where the first two peaks represent CO_2. The intensities of cyanogen, isocyanic acid and 3,4-dicyanofurazan have lower intensity in Region 1, with isocyanic acid and 3,4-dicyanofurazan producing peaks near background levels. These peaks likely represent more extensive breakdown of TATB into small molecules that occurs later in the thermal breakdown process as indicated by their prominence in Region 2 (Figure 5B).

Figures 5C and D show the later peaks in the chromatogram (7-17 min) are associated with masses ≥ m/z 177. Region 2 produced more intense peaks associated with thermal breakdown molecules when compared to Region 1. The TATB peak was variable in intensity and retention from sample to sample and produced poor chromatographic retention times ranging from 15.8 to 16 min. The contribution of the TATB molecular ion was greater in the early stages of thermal decomposition when regions 1 and 2 are compared, likely indicating more complete thermal breakdown of TATB driven by gas-phase reactions. The cryo-focused chromatography verified the known TATB thermal decomposition products occurring as TATB is dehydrated during heating. This process produces a furazan group on the TATB carbon ring as a water molecule is formed. There can be up to three furazan groups formed on TATB.

We observed F1, F2 and F3 formation during isothermal heating in a pseudo-confined environment. Additionally, we identified 2 compounds that have not been previously identified in the literature (F1 nitro loss and F3 ring opening). These compounds appear more in Region 2 and are likely linked to more complete breakdown of TATB into small molecules and gases ≤ m/z 120. Two of these compounds represent the loss of nitro functional groups from F1 and F2 during decomposition. The third compound results from the loss of oxygen from a furazan group on F3 leading to the opening of the carbon ring.

3.4 Identification of separated compounds

Figures 6 and 7 show the mass spectra of each compound identified. The mass spectra of TATB was verified with the NIST GC-MS database along with F3 and F2-nitro loss, with > 81% matches (Figure 6). The retention time of F1 overlapped with TATB in the chromatograph, which made acquiring a clean mass spectrum challenging (Figures 5 and 6B). However, the fragmentation patterns indicate that mass losses of 14, 16, 30, 52 and 120 are occurring which correspond to N, O, NO, NH_2, C_2N_2 and C_2N_2O. These mass differences correspond to the differences observed in other furazan compounds and verify the presence of F1. We identified novel compounds associated with TATB thermal breakdown representing the loss of nitro groups from furazans and the opening of the F3 ring structure. The F1 nitro loss compound has a molecular ion at 195 m/z which represents a mass loss of 45 m/z (Figure 6E). As this compound forms, a hydrogen atom would bond with the carbon ring exposed by the nitro group loss resulting in an +1 amu addition to the mass. When this

is considered a net mass loss of 46 m/z occurs, which is likely associated with the loss of a nitro group. The same process occurs with the F2 nitro loss compound with a shift from 222 m/z to 177 m/z, with a mass loss of 45 m/z (Figure 7A). This compound has been identified in previous studies [11, 24].

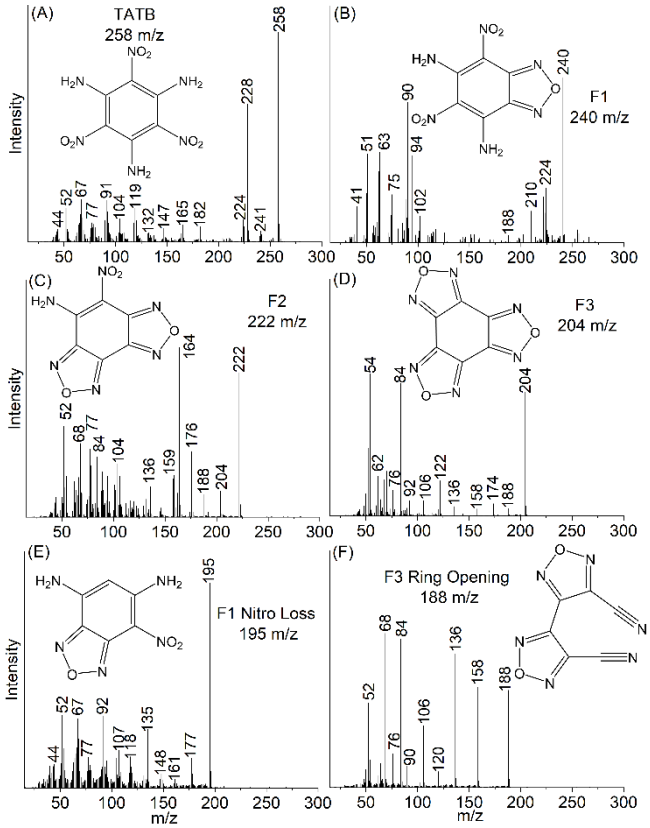

Figure 6. Mass spectra of compounds identified during isothermal heating of TATB. (A) TATB, (B) F1, (C) F2, (D) F3, (E) F1 nitro loss and (F) F3 ring opening.

The masses 52 and 120 correspond to cyanogen, and 3,4-dicyanofurazan (Figure 7 B and C), repectively. The cyanogen mass spectrum produced a 95% match in the NIST database, while 3,4-dicyanofurazan had an 80% match. Mass m/z 43 had a 95% NIST match with isocyanic acid (HNCO), However isofulminic acid (CNOH, hydroxyl group) could also result (Figure 7F). Compounds with masses < 120 m/z produced simple fragmentation patterns (Figure 7C - F). Masses 52, 44 (cyanogen and carbon dioxide) only produced a single mass spectrum peak with no fragmentation. Mass 43 (isocyanic acid) had a main peak at 43 m/z along with a peak at 42 m/z that represents a proton loss during (Figure 7F). A mass spectrum at with a retention time of 0.172 min was extracted and the contributions from the neighboring peaks from cyanogen and isofulminic acid were subtracted (Figures S4 and 7D). A peak at mass 46 was present and supports the formation of nitrogen dioxide gas in the thermal breakdown mechanism.

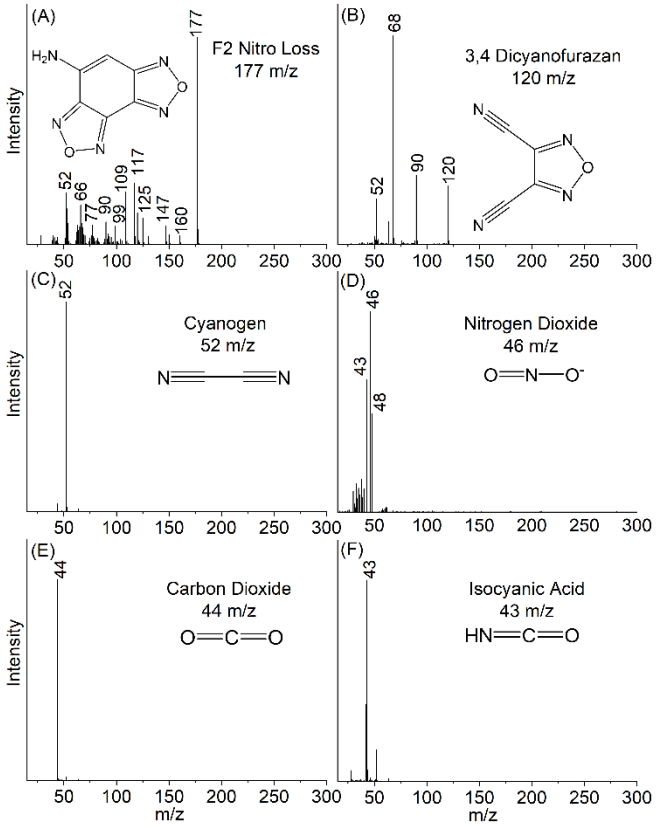

Figure 7. Mass spectra of compounds identified during isothermal heating of TATB continued. (A) F2 nitro loss, (B) 3,4 dicyanofurazan, (C) cyanogen, (D) nitrogen dioxide, (E) carbon dioxide and (F) isocyanic acid.

The loss of nitro functional groups during TATB thermal breakdown is an important finding because this could result in the release of nitrogen dioxide gas, which is a powerful oxidant [25]. While no distinct peaks in the TIC were associated with nitrogen dioxide (46 m/z), we did observe EICs in the first minute co-eluting with CO_2, cyanogen and isocyanic acid (Figure S4). The intensity of mass 46 was low and the EIC scale was increased in intensity 2000 times to observe the peaks. Nitrogen dioxide gas is highly reactive and is likely being consumed as TATB oxidizes and produces CO_2 (or N_2O). Additionally, the GC column used to separate the compounds has a 5%-phenyl-methylpolysiloxane stationary phase that is not suitable for the proper separation of molecular gases like CO_2, N_2 and NO_2. The masses and retention times for all compounds are listed in Table 1.

Table 1. Retention times for cryo-focused compounds formed during isothermal heating of TATB at 330°C

Mass	Retention Time (Min)	Formula	Compound
258	15.8-16	$C_6N_6O_6H_6$	TATB
240	15.764	$C_6N_6O_5H_4$	F1 (benzo-monofurazan)
222	13.387	$C_6N_6O_4H_2$	F2 (benzo-difurazan)
204	9.59	$C_6N_6O_3$	F3 (benzo-trifurazan)
195	12.998	$C_6N_5O_3H_5$	F1-NO_2 Loss
188	7.525	$C_6N_6O_2$	F3 Ring Open
177	11.481	$C_6N_5O_2H_3$	F2-NO_2 Loss
120	0.366	C_4N_4O	3,4-Dicyanofurazan
52	0.162	C_2N_2	Cyanogen
46	0.172	NO_2	Nitrogen Dioxide
44	0.131	CO_2	Carbon Dioxide
43	0.208	HNCO	Isocyanic Acid

4 Discussion

4.1 Sample cup design and implications towards submlimation and decomposition

The behavior of the TATB in these experiments reflects the sample cup design. The unconfined design yields spectra as a combination of sublimation (parent ion and fragments) and thermal decomposition (furazan thermal products) based on the distribution of masses. Figure 7A shows the fragment ions for the EI-MS of TATB. The masses compared to Table 1 clearly delineate the difference between the EI-MS of TATB and the thermal decomposition products of TATB. Particularly, the TATB mass spectrum shows an intense parent ion and minor fragmentation in the m/z < 120. The pseudo-confined sample cup accentuates the thermal decomposition products with minor or no contributions from sublimation. The parent ion of TATB is minimal using this sampling design. This is a critical distinction in establishing using MS to identify thermal decomposition products vs. fragments of the parent ion. Small molecules evolving during thermal decomposition can be easily confused with fragments of TATB in EI type spectra.

The pseudo-confined cup design reduces sublimation by restricting the exit orifice causing longer residence times in the cup (reactor), so decomposition reactions have a better chance to occur. This effect has been delineated previously in studies on TATB sublimation/thermal decomposition. Farber & Srivastava used a Langmuir (evaporation) and an effusion cell design to compare EI-MS of sublimation with decomposition of TATB [10]. Land et al. used different orifice sizes on a MS source to compare the same [11]. Recent work with DSC/TGA, which this work is aligned with, found 50-75 µm pinhole openings limited sublimation into the gas phase, allowing thermal decomposition processes and more accurate measurement of heat flow and enthalpy [23]. The T_{max} values for the constant heating rate experiments in this work show a difference between the unconfined and pseudo-confined samples to be about 4 °C at 10 °C/min indicating the lower sublimation temperature is affecting the overall evolution profile. This is even more evident in the isothermal conditions. The unconfined samples only partially decompose while most of the sample sublimes, so the mass is expended at around 15 min. In the pseudo-confined samples sublimation is minimized, so the profiles extend to much longer times as the decomposition reactions proceed.

The decomposition gases are associated with a range of furazan [11, 12, 24, 26, 27] and small molecule [8-14] reaction byproducts. The initial pulse of gases during the initial evolution in the isothermal cases is a combination of background gases from the septum purge, along with the rapid volatilization of the TATB impurities, T4A, and toluene remaining from the synthesis reactions [22] (Figure S3). The steady state release of gases during the first 1 to 10 min of isothermal heating of the pseudo-confined samples before the increase of evolved gases suggests a more complicated reaction sequence is occurring, which has been seen previously in SDT and hot stage FTIR isothermally treated sample [28].

4.2 Cryo-focused molecular separations

The intensity of the TATB molecular ion is greater, and the thermal decomposition products are less intense in the cryo-focused Region 1 than Region 2, indicating more extensive decomposition of TATB occurring later in the thermal breakdown process (Figures 4 and 5). This process produces furazan groups on the TATB carbon ring as a water molecule is formed. Three compounds indicate this chemistry (F1, F2, and F3).

This study also identified two novel compounds associated with TATB thermal decomposition. A small chromatographic peak at 12.998 min (Table 1 and Figure 5) resulted from the loss of a NO_2 group from F1 with a mass of 195. The loss of a NO_2 group from the F2 was also observed in this study (177 m/z) which confirms other studies [8, 11, 24]. A major peak associated with mass 188 appeared in the cryo-focused chromatograms of Region 2 with a retention time of 7.525 min. This molecule results from the loss of oxygen from the F3 molecule and opens the carbon ring. Likely this step allows further decomposition into small molecules ≤120 m/z. Another loss of oxygen from the F3-ring open molecule would result in the formation of 3,4-dicyanofurazan (120 m/z) and cyanogen (52 m/z).

4.3 Thermal decomposition implications

A significant delay in thermal decomposition and gas generation was observed during isothermal heating at 330°C under pseudo-confined conditions (Figure 2D). Previous TATB thermal decomposition studies focused on constant heating rate environments, however the isothermal experiments reveal there is a lag in decomposition and gas generation initially occurring when decomposition temperatures are reached. This is likely occurring due to overcoming kinetic energy barriers in order for auto-catalytic reactions to occur. These reactions are likely driven by the loss of nitro

functional groups, which generate oxidizing NO_2 gas. The weakest bond on TATB is predicted to be the nitro-carbon functional group [29, 30]. The thermal decomposition lag may be caused by the kinetic barriers to releasing NO_2 groups [30].

The verification of NO_2 loss in TATB thermal decomposition products along with a weak signal measured with various mass spec and vibrational spectroscopy techniques [10] suggests NO_2 molecule is highly reactive [25, 31-33] and may drive a portion of the TATB decomposition, resulting from a series of redox reactions, such as the oxidation of the carbon ring to CO_2 and drive the redox reactions aiding in the formation of furazans. The high reactivity may explain why it is only found in trace levels in the gas phase. Measurable amounts of NO have been observed in other studies [8, 9, 11, 12, 24] and may also participate in redox reaction by reacting with O_2 to form NO_2 gas [25, 31, 34]. The NO gas may also be acting as a reducing agent as furazans form, with NO gas reacting to reduce nitrogen from NO_2 groups, and NO_2 gas reacting to oxidize amine groups as furazans form. Intramolecular electron transfer may also be driving this redox balance as furazans are formed [33]. Overall, these results suggest an auto-oxidation mechanism driven by NO_2 gas formation is a strong driver of TATB thermal decomposition.

4.4 Comparison to other studies

The characterization of TATB thermal decomposition products on the molecular level has been of interest because of implications in safe handling [15, 35]. Most studies propose furazans, furoxans and light-gases evolving, based on decomposition products. Farber and Srivastava examined TATB with EI-MS used different size apertures on sample cells to distinguish between parent ion/fragments and decomposition products [10]. Several species with m/z values lower than TATB have been reported in the literature, indicating compounds formed by ring opening, as well as light gases such as NO_2, CO_2, and NO. Catalano and Rolon treated TATB isothermally in the range of 200 to 312 °C under confinement, analyzed the products by matrix isolation IR and gas analyses MS, and found several light gases, CO_2 and H_2O, including oxides of nitrogen; C_2N_2 and HCN were only observed when the samples deflagrated [9, 13]. Furazans and furoxans were not mentioned even in the non-volatile residues generated from ODTX residual samples. Using x-ray photoelectron spectroscopy (XPS), Sharma et al. studied several residues generated from shock, irradiation, and thermal exposure conditions in a small reaction cell [36]. The furazan reaction sequence of F_1, F_2, and F_3 was proposed based on the observation of x-ray photoelectron spectroscopy shifts in N1s positions with C1s and O1s positions. The loss of NO_2 on F_2 was also reported.

In a series of extremely fast pyrolysis experiments from RT to 500 °C (T-jump) on TATB, Brill and James report several light gases formed using FTIR analyses, including HCN, HNCO, and N_2O [37]. Using STMBMS (simultaneous thermogravimetric modulated beam MS with time-of-flight detection) with different cell designs, Land et al. [11] clearly detected the formation of furazans and light gases temporally resolved when TATB was heated. The size of the orifice in the cell dictated the species by MS detection whether they were sublimation/fragments or thermal decomposition products. Again, the furazan decomposition sequence was observed as well as some light gases, including C_4N_4O and C_2N_2.

In a series of papers, Belmas et al. studied the results of T2 (French version of polymer bonded TATB) subjected to isothermal TGA at temperatures 200 to 330 °C [12, 38]. Light gases were observed evolving, such as HCN, N_2, CO_2, and C_2N_2. The residues were also examined by extraction with CH_3CN showing F1 and F2, but no F3 was detected. Carter et al. examined residues of pyrolyzed TATB with various spectroscopic techniques and found the residue is an integration of amorphous carbon and C-N bonded species, including ring systems [39]. More recent improvements of analytical techniques have led to expanding the network of compounds. Kahl et al. using extraction, separation with optical (HPLC-DAD) and MS (HPLC-MS) detection techniques on small-scale cook-off residues to show more compounds structurally related to TATB, such as mono-nitroso-TADB (MN-TADB) and hydroxyl-TATB (HO-DATB), are involved in addition to the furazan network [14].

Reynolds et al. expanded the list of compounds when examining the residues from a suite of partially confined cook-off samples by HPLC-DAD and HPLC-MS to include several unidentified compounds eluting in DMSO extracts [14, 26]. The residues were also examined by solid-state NMR which exhibited evidence of primarily sp^2 C with C-N incorporation. Koroglu et al. using *in-situ* FTIR to examine TATB and d_6-TATB degraded in isothermal conditions, found a significant kinetic isotope effect in the evolution of light gases, even in gases not containing N, such as CO_2 [8]. Burnham et al. using HPLC-DAD techniques showed the evolution of several species with TATB-like structures being produced and then consumed during small-scale isothermal experiment at 330 °C [28]. These species include F1, F2, and newly recognized hydroxyl F_1 (HO-F1), along with several other unidentified compound with m/z of 200 and higher. Coffee et al., expanded the list of detected compounds from the same set of samples to include imidazole-TATB, HO-F2, triazole-TATB, nitrile-TATB and others [27]. In addition, proposed several structures of products with m/z greater than TATB. A compilation of the known molecules associated with TATB decomposition (thermal, shock, radiation) is listed in Table 2.

5 Conclusions

The results from this study provided the first cryo-focused chromatographic separation of TATB thermal decomposition products, including the verification of known products along with the discovery of two novel molecules. Specifically, the discovery of an open ring F3 structure suggests that the loss of oxygen from F3

results in the un-zipping of the furazan ring and leads to the formation of other lower molecular weight products (≤ 120 m/z). The loss of nitro groups from furazans was also observed and our results also show this occurs on the F1 furazan as well. The loss of nitro groups may be associated with the release of nitrogen dioxide gas, a powerful oxidant, that could oxidize TATB. These results are important for the proper modeling of HE thermal decomposition as it relates to HE that has been subject to off normal heating events (e.g. fires, slow cookoff) and the safe handling of explosives.

Table 2. Molecules associated with TATB decomposition

Mass	ions	Reference/Comments	Mass	ions	Reference/Comments
2	H_2	[9, 10, 13, 24, 40]	176	unassigned	[11]
16	O, CH_4,	[9, 13, 24]	177	$C_5N_5O_2H_3$	[11, 24][This Study], F2 minus NO2
17	OH, NH_3,	[8, 11, 24, 40, 41]	**188**	**$C_6N_6O_2$**	[This Study], F3 ring open
18	H_2O	[8-13, 24, 40, 41]	**195**	**$C_6N_5O_3H_5$**	[This Study], F1 minus NO2
24	unassigned	[40]	204	$C_6N_6O_3$	[11, 26, 42][This Study], F3
25	unassigned	[40]	207	$C_6HN_5O_4$	[40]
26	CN	[40]	213	$C_6H_7O_4N_5$	[14, 22, 27], T3A snthesis impurity
27	HCN	[8, 9, 11-13, 24, 40-42]	220	$C_7H_4O_3N_6$	[14, 26, 27], NC-TATB
28	CO, N_2	[8-10, 12, 13, 24, 40, 41]	222	$C_6N_6O_4H_2$	[11, 14, 26, 27, 42][This Study], F2
30	NO	[8-13, 24, 40, 41]	223	$C_6HO_5N_5$	[27], HO-F2
43	HNCO	[8, 11, 24, 40, 41][This Study]	225	$C_6H_3O_5N_5$	[27], F1-T3A
44	CO_2, N_2O	[8-13, 24, 40, 41][This Study]	225	$C_6H_5O_4N_6$	[27], Triazole-TATB
46	NO_2	[10][This Study]	238	$C_6N_6O_5H_2$	[26], F1X1
52	C_2N_2	[9, 11-13, 24, 40, 41][This Study]	238	$C_7H_6O_4N_6$	[27], Imidazole-TATB
58	$(CH_3)_2C=O$	[9, 13]	240	$C_6H_6O_5H_4$	[11, 14, 26, 27, 42][This Study], F1
68	C_2N_2O	[9, 11, 13, 24, 40]	241	$C_6H_3O_6N_5$	[27], HO-F1
70	C_2NO_2	[10]	242	$C_6H_6O_5N_6$	[14, 26, 27, 42], MN-TATB
86	$C_3N_2O_2H_2$	[10]	244	$C_{13}H_{24}O_4$	[27]
96	$C_4N_2H_2O$	[22]	247	$C_6H_6O_4N_5Cl$	[14, 26, 27, 42], T4A
98	$C_3N_2O_2H_2$	[10]	256	$C_6H_4O_6N_6$	[26, 42][25, 40], FX1
101	unassigned	[40]	258	$C_6H_6O_6N_6$	[14, 26, 27, 42][This Study], TATB
110	$C_4N_2H_2O_2$	[22]	259	$C_6H_5O_7N_5$	[14, 26, 27], HO-TATB
114	$C_3H_3O_2H_4$	[10]	273	$C_9H_3O_4N_7$	[27]
119	$C_6N_2OH_3$	[11, 24]	278	$C_{16}H_{22}O_4$	[27]
120	C_4N_4O	[11, 24, 40][This Study]	282	$C_8H_6O_4N_6S$	[27], DMSO product
125	$C_4HN_2O_3$	[40]	283	$C_{10}HO_4N_7$	[27]
128	$C_3N_2O_4$	[10]	324	$C_{11}H_4O_3N_{10}$	[27]
131	multiple	[40]	330	$C_{17}H_{28}N_7$	[27]
144	$C_3N_3O_2H_2$	[10]	339	$C_{12}H_5O_4N_9$	[27]
147	$C_6N_4OH_3$	[11]	366	$C_{12}H_2O_5N_{10}$	[27]
155	$C_4HN_2O_3$	[40]	384	$C_{12}H_4O_6N_{10}$	[27]
156	$C_4H_4N_4O_3$	[40]	402	$C_{12}H_6O_7N_{10}$	[27]
164	unassigned	[11]	403	$C_{12}H_7O_7N_{10}$	[27]
169	unassigned	[40]			

(a) Farber & Srivastava, 1981 [10]; (b) Catalano & Rolon, 1983a & 1983b [9, 13]; (c) Land et al., 1993 [11]; (d) Belmas et al., 2004 [12]; (e) Yancey et al., 2018 [24]; (f) Coffee et al., 2022 [22]; (g) Yancey et al., 2020 [41]; (h) Loughran et al., 1977 [40]; (i) Coffee et al., 2023 [27]; (j) Reynolds et al. 2021 [26]; (k) Kahl et al., 2020 [14]; (l) Kahl et al., 2018 [42]; (m) Koroglu et al.,2021 [8].

Acknowledgements

This work was performed under the auspices of the U.S. Department of Energy by Lawrence Livermore National Laboratory under Contract DE-AC52-07NA27344.

References

[1] P. Folly, *Chimia* **2004**, *58*, 394-400.

[2] G. H. Miller, P. S. Brown, C. T. Alonso, Lawrence Livermore National Laboratory, UCRL-53822, **1987**, OSTI Report 6032983.pdf.

[3] C. L. Jackson and J. F. Wing, Proc. Am. Acad. Arts Sci. **1887**, *23* (1), 138-148; C. L. Jackson and J. F. Wing, On Benzo-tri-sulfonic acid, *J. Am. Chem. Soc.* **1887**, *9*, 324-355; C. L. Jackson and J. F. Wing, On Tribromotrinitrobenzol, *J. Am. Chem. Soc.* **1888**, *10*, 283-294 (1888).

[4] H. H. Cady, A. C. Larson, *Acta Crystallogr.* **1965**, *18*, 485–496, DOI: 10.1107/S0365110X6500107X.

[5]. T. Han, P. Pagoria, A. Gash, A. Maiti, C. Orme, A. Mitchell, L. Fried, *New J. Chem.* **2009**, *33*, 50–56, DOI: 10.1039/b810109d.7.

[6] B. A. Steele, S. M. Clarke, M. P. Kroonblawd, I. F. W. Kuo, P. F. Pagoria, S. N. Tkachev, J. S. Smith, S. Bastea, L. E. Fried, J. M. Zaug, E. Stavrou, O. Tschauner, *Appl. Phys. Lett*. **2019**, *114*, 191901-5, DOI: 10.1063/1.5091947.

[7] C. Wu, L. Fried, J. Phys. Chem. A **2000**, *104*, 6447-6452.

[8] B. Koroglu, J. C. Crowhurst, E. M. Kahl, J. S. Moore, A. Racoveanu, H. E. Mason, D. G. Weisz, J. G. Reynolds, A. K. Burnham, *Propellants, Explos., Pyrotech*. **2021**, *46*, 1352-1366, DOI: 10.1002/prep.202100082.

[9] E. Catalano, C. E. Rolon, *Thermochim. Acta* **1983a**, *61*, 37-51.

[10] M. Farber, R. D. Srivastava, *Combust. Flame* **1981**, *42*, 165-171, DOI: 10.1016/0010-2180(81)90155-3.

[11] T. A. Land, W. J. Siekhaus, M. F. Foltz, R. Behrens Jr., *Proceedings of the 10th Detonation Symposium, International*, Boston, MA, **1993**, 181-189.

[12] R. Belmas, A. Bry, C. David, L. Gautier, A. Keromnes, D. Poullain, G. Thevenot, C. Le Gallic, J. Chenault, G. Guillaumet, *Propellants, Explos., Pyrotech.* **2004***, 29* (5) 282-286, DOI: 10.1002/prep.200400059.

[13] E. Catalano, C. E. Rolon, *Thermochim. Acta* **1983b**, *61*, 53-71, DOI: 10.1016/0040-6031(83)80302-5.

[14] E. M. Kahl, N. K. Muetterties, A. J. Nelson, H. E. Mason, J. V. Crowhurst, K. R. Coffee, J. S. Moore, J. G. Reynolds, *AIP Conference Proceedings* **2020**, *2272*, 050010, DOI: 10.1063/12.0000948.

[15] S. F. Rice, R. L. Simpson, Report UCRL-LR-103683, Lawrence Livermore National Laboratory, Livermore CA, 94550, USA July 4, **1990,** DOI: 10.2172/6426268.

[16] J. Sharma, J. C. Hoffsommer, D. J. Clover, C. S. Coffey, F. Santiago, A. Stolovy, S. Yasuda, *Shock Waves in Condensed Matter* (Eds.: J. R. Asay, R. A. Graham, G. K. Straub), Elsevier, Amsterdam **1983**, pp 543-546, DOI: 10.1016/B978-0-444-86904-3.50123-8.

[17] J. Yinon, R. A. Yost, S. Bulusu, Thermal Decomposition Characterization of Explosives by Pyrolysis-Gas Chromatography-Mass Spectrometry, *J. Chromatogr. A* **1994**, *688*, 231-242.

[18] K. Tei, M. Matsueda, K. Matsui, T. Ishimura, A. Watanabe, W. Pipkin, N. Teramae, H. Ohtani, C. Watanabe, *J. Anal. Appl. Pyrolysis* **2022**, *168*, 105707, DOI: 10.1016/j.jaap.2022.105707.

[19] J. S. Moore, A. K. Burnham, K. D. Morrison, Keith R. Coffee, B. Koroglu, G. L. Klunder, A. Racoveanu, J. G. Reynolds, Lawrence Livermore National Laboratory report JRNL-853838, submitted to *Propellants, Explos., Pyrotech*. **2023**, prep.202300237, August.

[20] T. M. Benziger, *Method for the Production of High-Purity Triaminotrinitrobenzene*, US Patent, 4032377, **1977**, June 28.

[21] A. K. Nandi , S. M. Kasar , U. Thanigaivelan , M. Ghosh, A. K. Mandal, S. C., *J. Energ. Mater.* **2007,** *25:4*, 213-231, DOI: 10.1080/07370650701567066.

[22] K. R. Coffee, A. F. Panasci-Nott, B. J. Stewart, J. A. Olivas, A. M. Williams, J. G. Reynolds, *Propellants, Explos., Pyrotech.* ***2022***, e202100224, DOI: org/10.1002/prep.202100224.

[23] B. Koroglu, A. K. Burnham, I. Mashiana, A. Racoveanu, C. Arose, C. J. Crowhurst, J. G. Reynolds, *Propellants, Explos., Pyrotech.* **2023**, *48*:e202300124, 1-13, DOI: 10.1002/prep.202300124.

[24] B. J. Yancey, N. K. Muetterties, E. M. Kahl, E. A. Glascoe, J. G. Reynolds, *Proceedings of the 16th International Detonation Symposium*, **2018**, ONR-43-5762-19, 1664-1675.

[25] F. A. Villamena, "Chapter 2 - Chemistry of Reactive Species" in Reactive Species Detection in Biology, F. A. Villamena, Ed. (Elsevier, Boston, 2017), pp. 13-64.

[26] J. G. Reynolds, N. K. Muetterties, A. J. Nelson, H. E. Mason, J. S. Moore, K. R. Coffee, E. M, Kahl, *Propellants, Explos., Pyrotech.* **2021**, *46*, 1-15, DOI: prep.2021.00034.

[27] K. R. Coffee, A, F. Panasci-Nott, J. A. Olivas, J. Selinsky, K. D. Morrison, A. K. Burnham, G. L. Klunder, and J. G., Lawrence Livermore National Laboratory report, LLNL-JRNL-850998, 23-S-2556 available Lawrence Livermore National Laboratory, accepted for publication, *Propellants, Explos., Pyrotech.* **2023***,* prep.202300176.

[28] A. K. Burnham, K. R. Coffee, G. L. Klunder, A. F. Panasci-Nott, J. G. Reynolds, Lawrence Livermore National Laboratory report, LLNL-JRNL-848399 available Lawrence Livermore National Laboratory, accepted for publication *Propellants, Explos., Pyrotech.* **2023** prep.202300121.R1.

[29] A. Stephen, P. Srinivasan, P. Kumaradhas, *Comput. Theor. Chem*. **2011**, 967, 250-256, DOI: 10.1016/j.comptc.2011.04.026.

[30] B. A. Steele, *J. Appl. Phys.* **2023**, *133*, 075902, DOI: 10.1063/5.0139625.

[31] M. Bartberger, W. Liu, E. Ford, K. Miranda, C. Switzer, J. Fukuto, P. Farmer, D. Wink, K. Houk, *Proc. Natl. Acad. Sci. U. S. A.* **2002**, *99*, 10958-10963, DOI: 10.1073/pnas.162095599.

[32] J. R. Lancaster, *Future Sci OA* **2015**, *1*, FSO59, DOI: 10.4155/fso.15.59.

[33] K. D. Morrison, A. Racoveanu, J. S. Moore, A. K. Burnham, B. Koroglu, K. R. Coffee, A. F. Panasci-Nott, G. L. Klunder, B. A. Steele, M. A. McClelland, J. G. Reynolds, *Scientific Reports* **2023**, *13*, 21256. https://doi.org/10.1038/s41598-023-47952-6.

[34] J. A. Last, W.-M. Sun, H. Witschi, *Environ. Health Perspect*. **1994**, *102*, 179–184, DOI: 10.1289/ehp.94102s10179.

[35] B. M. Dobratz, Los Alamos National Laboratory report, LA-13014-H, **1995**, August, DOI: 10.2172/90370.

[36] J. Sharma, W. L. Garrett, F. J. Owens, V. L. Vogel, *J. Phys. Chem*. **1982**, *86*, 1657-1661, DOI: 10.1021/j100206a034.

[37] T. B. Brill, K. J. James, *Chem. Rev.* **1993**, *93*, 2667–92, DOI: 10.1021/cr00024a005.

[38] R. Belmas, L. Gautier, C. David, D. Picart, C. Le Gallic, P. Lambert, *Propellants, Explos., Pyrotech.* **2005**, *30*, 101–104, DOI: 10.1002/prep.200400090.

[39] J. A. Carter, J. M. Zaug, A. J. Nelson, M. R. Armstrong, M. R. Manaa, *J. Phys. Chem. A* **2012**, *116*, 4851–4859, DOI: 10.1021/jp301771y.

[40]. Loughran, E. D., Wewerka, E. M., Rogers, R. N. & Berlin, J. K., Los Alamos National Laboratory report, LA-6873-MS, (1977).

[41] B. J. Yancey, E. A. Glascoe,E. M. Kahl, P. F. Pagoria, J. G. Reynolds, LLNL Technical report, LLNL-TR-833774, available at Lawrence Livermore National Laboratory, 7000 East Ave., Livermore CA 94550 (2020).

[42] E. M. Kahl, P. C. Hsu, K. R. Coffee, B. J. Yancey, A. J. Nelson, H. E. Mason, G. F. Ellsworth, T. E. Healy, J. C. Crowhurst, T. W. Myers, J. G. Reynolds, *Proceedings of the 16th Detonation Symposium, International*, 2018, ONR-43-5762-19, **2018**, 1642-1652, LLNL-PROC-754001.